IEICE TRANS. COMMUN., VOL.E93–B, NO.6 JUNE 2010

PAPER

A CFAR Circuit with Multiple Detection Cells for Automotive UWB Radars

Satoshi TAKAHASHI[†a)], ***Member***

SUMMARY Future high-resolution short-range automotive radar will have a higher false alarm probability than the conventional low-resolution radar has. In a high-resolution radar, the reception signal becomes sensitive to the difference between intended and unintended objects. However, automotive radars must distinguish targets from background objects that are the same order of size; it leads to an increase in the false alarm probability. In this paper, a CFAR circuit for obtaining the target mean power, as well as the background mean power, is proposed to reduce the false alarm probability for high-resolution radars working in automotive environments. The proposed method is analytically evaluated with use of the characteristic function method. Spatial correlation is also considered in the evaluation, because the sizes of the both target and background objects approach the dimension of several range cells. Result showed the proposed CFAR with use of two alongside range cells could reduce the ratio of 6.4 dB for an example of an automotive situation.

key words: *automotive radar, radar clutter, CFAR, automatic target detection, spatial correlation*

1. Introduction

The first automotive radars for potential accident decrease and for autonomous cruise control were available in 1999, and 77-GHz band long-range radars and 24-GHz band short-range radars have been developed in Europe [1]. The wide sense ultra wideband (UWB) include a broadband radio such as the high-resolution radar (HRR). The 24-GHz band is temporally granted and will be superseded by the 79-GHz band until mid 2013. Short-range automotive radars in the 79-GHz band will have a bandwidth of 4 GHz, and are expected to have a maximum range of 30 m and a range resolution of 5 cm.

In general, reception radar signals contain echoes from undesired background objects, and these echoes often make it difficult to find out the targets. Undesired radar echoes, called *radar clutter*, are suppressed with the target and clutter characteristics and by using electrical circuitry of signal processing of space and time. For example, meteorological radars use moving target indication (MTI) to suppress clutter comes from terrain [2]. A meteorological radar typically works at a frequency of 5-GHz band has a pulse width of around 1 μs. The size of raindrops is significantly smaller than the size of the wavelength and the radar resolution, but the size of terrain is significantly larger than them. Therefore, rain echoes vary and terrain echoes are steady. Because of the pulse-to-pulse power-variation differences at a certain range cell, MTI significantly suppresses terrain clutter.

Radars for predicting near misses or intrusions need an automatic target detection. Automatic target detection applying a fixed threshold to the radar signal often triggers false alarms. A 1-dB change in the threshold can results in three orders of magnitude change in the false alarm probability [2]. An increase in the threshold leads to a lower false alarm, but it results in a lower detection probability. Undesired background objects having high reflectivity increase the mean reception power, and therefore they causes a higher false alarm. The adaptive threshold determination circuitry, called constant false alarm rate (CFAR, pronounced as "*sea far*"), was proposed [3]. A CFAR circuit uses amplitudes of several range cells around the interest cell to adjust the threshold adaptively. An abrupt strong signal from background object leads to overestimation of the threshold, because the determination is based on averaging of alongside cells. To solve the problem, there are variations of a CFAR circuit, including smallest-of (SO) CFAR [4], ordered-statistics (OS) CFAR [5], and and-or CFAR [6], and they have been examined for automotive radars [7].

An increase in a radar resolution results in a higher peak-to-average power ratio in the reception signal, then the signal is referred to as spiky. For example, maritime radars, working at a 9-GHz band with a pulse width of several tens ns, would meet echoes from many sea surface facets within the radar resolution. The resulting signal obeys Rayleigh distribution and then the CFAR circuit works well. With an HRR, however, a few facets contribute the resulting signal, and the signal varies range-by-range, which characterize spiky clutter [8]. Then, the sizes of ships and terrain are larger than the radar resolution, but the size of the sea surface facets is approaching the same dimension of the radar resolution. Then, the target signal would not vary, and the amplitude variation of clutter has been modeled as Weibull distribution, log-normal distribution, and K-distribution by results of many measurements. There are variations of CFAR circuits for these distribution assumptions, including nonparametric detector [9] and Weibull CFAR [10].

They assumed the target signal strength did not vary while pulse-to-pulse and scan-to-scan. However, the target signal strength would vary on HRRs in automotive environments, because the orders of targets, clutter, and the radar resolution are the same, and it increases the false alarm probability. In this paper, a variation of a CFAR circuit that measures local mean powers of both target and clut-

Manuscript received September 2, 2009.
Manuscript revised December 26, 2009.

[†]The author is with the Faculty of Information Sciences, Hiroshima City University, Hiroshima-shi, 731-3194 Japan.
a) E-mail: s.takahashi@m.ieice.org

DOI: 10.1587/transcom.E93.B.1574

ter is proposed. Spatial correlation is introduced to evaluate performance of the proposed method, because target and clutter would occupy several range cells and spatial correlation increases a required target signal power for detection. Descriptions of a fundamental CFAR circuit, problems on high-resolution automotive radars, power distribution models for the target and clutter, and introduction to spatial correlation are provided in Sect. 2. The proposed CFAR is shown in Sect. 3, and the numerical result is given in Sect. 4.

2. Target Detection with Automotive UWB Radars

2.1 Fundamental CFAR

Here, we define the false alarm probability P_{F} as the probability the radar wrongly detects a target though a target does not exist at a single range cell. The detection probability P_{D} is the probability the radar detects a target when a target exists[†].

First, we consider a false alarm probability of the single pulse threshold detection where there is no target. Radiowaves from many background objects within the radar resolution interfere mutually. According to the central limit theorem, the resulting amplitude distribution of the pulse-to-pulse variation follows complex Gaussian distribution for coherent detection and obeys Rayleigh distribution

$$p(x) = \frac{2x}{\sigma^2}\exp\left(-\frac{x^2}{\sigma^2}\right), \tag{1}$$

for incoherent detection, where σ is the root mean squared amplitude. The probability that exceed a threshold x_{th} is

$$P_{\mathrm{F}} = \int_{x_{\mathrm{th}}}^{\infty} p(x)\,dx = \exp\left(-\frac{x_{\mathrm{th}}^2}{\sigma^2}\right). \tag{2}$$

Therefore, P_{F} increases as an increase in σ.

Figure 1 shows a fundamental CFAR circuit referred to as cell-averaging (CA) CFAR [3]. We assume the number of the reference cells is infinity, then we get the ensemble mean of clutter cells as

$$\langle x\rangle = \int_0^{\infty} x\,p(x)\,dx = \frac{\sqrt{\pi}}{2}\sigma. \tag{3}$$

The probability that CFAR output $\hat{x} = x - k\langle x\rangle$ exceeds zero is

$$P_{\mathrm{F}} = \int_{k\langle x\rangle}^{\infty} p(x)\,dx = \exp\left(-\frac{k^2\pi}{4}\right), \tag{4}$$

which does not depend on σ, and the false alarm probability becomes constant. An increase in k reduces P_{F} but also reduces P_{D}.

2.2 High-Resolution Radars and Automotive Radars

Variation at a cell is the superposition of time-to-time variation on range-by-range variation. If we average the successive radar pulses at each range cell, the time-to-time variation at the cell reduces. The procedure is called *pulse integration*, and it reduces the false alarm probability. In this paper, we consider radar signal in pulse-integrated power, not amplitude, because the power of a cell that consists of both target and clutter is the superposition of their powers under the independent assumption of them.

For low-resolution radars, the resolution is smaller than the size of the background objects, but is larger than the targets. If the background objects are uniformly distributed in the space we are interested in, the target detection is easy as explained in Fig. 2(a). As the resolution improves and the resolution approaches to the size of the background objects, the range-by-range variation becomes large, because the radar reception signal depends heavily on the object shape as shown in Fig. 3. The higher resolution increases the false alarm probability as shown in Fig. 2(b).

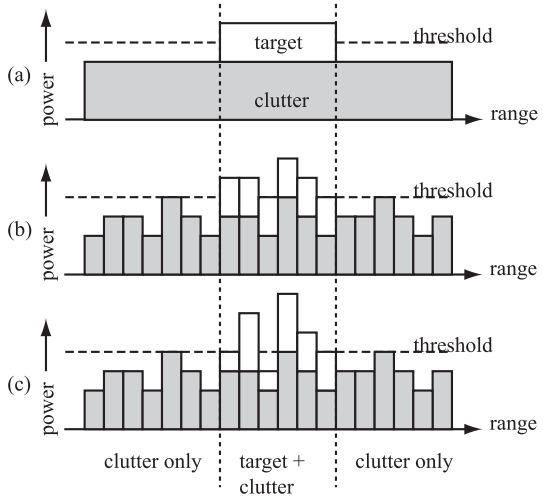

Fig. 2 Radar reception signal with (a) a low-resolution radar, (b) an HRR, and (c) an automotive HRR after pulse integration.

[†]Though effects of correlation on the probabilities of multiple cells statistics are discussed later, correlation does not effect on the single cell statistics.

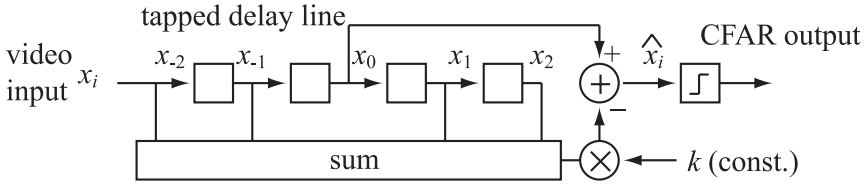

Fig. 1 A fundamental CFAR circuit.

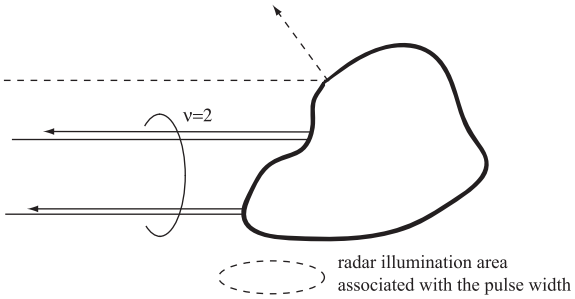

Fig. 3 Range-by-range power variations in an HRR with a change in the number of scattering centers in the same range bin.

For an HRR working in automotive environment, the dimensions of target, background objects, and the radar resolution are the same. Then, not only clutter but also target signals vary range-by-range, and it leads to an extra increase in the false alarm probability as explained in Fig. 2(c).

2.3 Reception Power Distribution

Though few papers have reported on the statistical power variations of an automotive HRR, an experimental result of an intervehicle HRR showed spiky reception signal [11]. According to studies on laser speckle patterns, the statistics of the spiky power variation has modeled as gamma distribution [12]. A partial illumination of radiowaves to an object is depicted in Fig. 3. The radar illumination area is determined by the pulse width, the resultant power in a range bin depends on the number of scatterer on the object. Because of roughness of an object, the power variation increases as a decrease in the radar illumination area. Measurement results on synthetic aperture radars (SAR) [13], [14] and a maritime radar [15] showed the power statistics of foliage, terrain, and sea followed a gamma distribution.

A gamma distribution is characterized by the shape parameter ν ($0 < \nu$) and the scale parameter β ($0 < \beta$), and ν is interpreted as the number of scattering centers in the same range bin. A lower ν (say, less than 3) leads to a spiky signal. Superposition of time-to-time exponential power variation (or Rayleigh amplitude variation) on range-by-range gamma power variation is known as the K-distribution variation [8]. For automotive radars, a target power, as well as clutter power, would obey a gamma distribution, and the power variation increases the required signal-to-clutter power ratio (SCR).

A probability density function (pdf) that obeys gamma distribution is expressed as

$$p(x) = \frac{x^{\nu}}{\Gamma(\nu)\beta^{\nu}} \exp\left(-\frac{x}{\beta}\right) u(x), \tag{5}$$

where $u(\cdot)$ is the unit step function [16]. The statistics of gamma-distributed random variable (RV) x are

$$\langle x \rangle = \nu\beta, \quad \mathrm{var}\,(x) = \nu\beta^2, \tag{6}$$

where $\langle x \rangle$ is the ensemble mean and $\mathrm{var}\,(x)$ shows the variance of x. Therefore, we obtain

$$\nu = \frac{\langle x \rangle^2}{\mathrm{var}\,(x)}, \quad \beta = \frac{\mathrm{var}\,(x)}{\langle x \rangle}. \tag{7}$$

2.4 Spatial Correlation

For RVs $x_1, x_2, \ldots, x_n$, the correlation coefficient ρ_i is expressed as

$$\rho_{j-i} = \frac{\langle (x_j - \bar{x})(x_i - \bar{x}) \rangle}{\langle (x_i - \bar{x})(x_i - \bar{x}) \rangle} = \frac{\langle (x_j - \bar{x})(x_i - \bar{x}) \rangle}{\mathrm{var}\,(x)}, \tag{8}$$

where $\bar{x} = \langle x \rangle$.

According to the reproductive property of a gamma distribution, the sum of n independent gamma RVs with the shape parameter of ν and the scale parameter of β becomes a gamma distribution with the shape parameter of $n\nu$ and the scale parameter of β. For correlated gamma RVs, the sum distribution also follows a gamma distribution by the idea of equivalent independent RVs [17]. The idea was introduced to analyze the performance of the pulse integration techniques for detection of a varying target.

When the gamma RVs $x_1, x_2, \ldots, x_n$ are correlated, the sum of the variance and mean depends on their correlation: the mean and variance are [18]:

$$\begin{aligned} &\langle x_1 + x_2 + \cdots + x_n \rangle \\ &\quad = \langle x_1 \rangle + \langle x_2 \rangle + \cdots + \langle x_n \rangle \\ &\quad = n\langle x \rangle, \end{aligned} \tag{9}$$

$$\begin{aligned} &\mathrm{var}\,(x_1 + \cdots + x_n) \\ &\quad = \langle \{(x_1 - \bar{x}) + \cdots + (x_n - \bar{x})\}^2 \rangle \\ &\quad = \mathrm{var}\,(x) \left\{ n + 2 \sum_{i=1}^{n-1} (n-i)\rho_i \right\}. \end{aligned} \tag{10}$$

3. Proposed CFAR with Multiple Target Detection Cells

Applying CFAR idea to radar signals after pulse integration is also possible. If we average alongside range cells whose number is corresponded to the possible target size (but it results in degradation of the original resolution), the number of radiowaves increases, and it would result in decrease in the required SCR.

A higher range resolution is preferable for precise locating such as parking, but the highest range resolution does not always help a driver to cruise roads (as a driver may not always use headlights with the high beam). The proposal coarse ranging, as an alternate of the fine ranging the original UWB radar has, can detects a weaker target with use of the original radar resolution.

The block diagram of the proposed CFAR is shown in Fig. 4. The series of the radar video inputs x_i are squared to express them in the powers, and the series of powers y_i are fed into the tapped delay line of $(m+1)$ cells. The base index y_0 is corresponded to the cell of interest. These cells assume to be integrated by many successive pulses (the integration

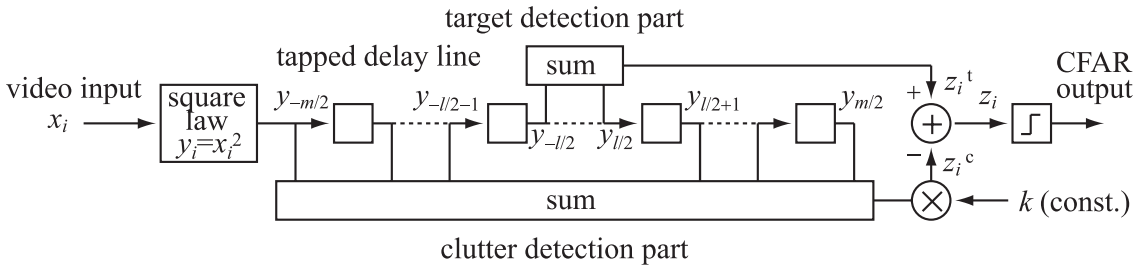

Fig. 4 Proposed CFAR.

circuit is not shown in the figure) to remove time-to-time variation and to improve the detection performance. There are two detection parts of target and clutter: the clutter detection part of $(m - l)$ cells calculates the local mean power as the conventional CFAR, and the target detection part of $(l + 1)$ cells extracts the target mean power. For example, $m = 20$ and $l = 2$ means there are 3 cells for the target detection, 18 cells for the clutter detection, and 21 cells in total.

For analysis of P_F and P_D of the proposed CFAR, the characteristic function (chf) method and its Fourier expansion form are used for expressing the reception power distribution. The power limited Fourier expansion is proposed [19]. Bandwidth-limited chf of the original pdf $p(x)$ is

$$\Phi(\omega) = \int_{-\infty}^{\infty} p(x)\, e^{j\omega x}\, dx \approx \int_{-R}^{R} p(x)\, e^{j\omega x}\, dx \tag{11}$$

where ω is an auxiliary variable and R is the maximum value of RV, and its Fourier series expansion can efficiently get the pdf from the chf [19]. The pdf can be calculated from the chf with the modified inverse Fourier transform [16],

$$p(x) = \frac{1}{2\pi} \int_{-\infty}^{\infty} \Phi(\omega)\, e^{-j\omega x}\, d\omega, \tag{12}$$

Though Eq. (12) involves the infinite-range integral, the distribution can efficiently be obtained because the reception power is not infinity. On the other hand, a pdf $p(x)$ can be expressed by

$$p(x) = \sum_{n=-\infty}^{\infty} p_n \exp\left(j\frac{n\pi}{R}x\right), \tag{13}$$

where p_n is the Fourier series,

$$p_n = \frac{1}{2R} \int_{-R}^{R} p(x) \exp\left(-j\frac{n\pi}{R}x\right) dx. \tag{14}$$

Comparing Eqs. (11) and (14), we obtain

$$p_n = \frac{1}{2R}\Phi\left(-\frac{n\pi}{R}\right). \tag{15}$$

Substituting Eq. (15) into Eq. (13), we get generic form of the pdf provided in [19]:

$$\begin{aligned} p(x) &= \frac{1}{2R} \sum_{n=-\infty}^{\infty} \Phi\left(\frac{n\pi}{R}\right) \exp\left(-j\frac{n\pi}{R}x\right) \\ &= \frac{1}{2R}\left[1 + 2\sum_{n=1}^{\infty} \mathrm{Re}\,\left\{\Phi\left(\frac{n\pi}{R}\right)\right\} \cos\frac{n\pi}{R}x \right. \\ &\quad \left. + 2\sum_{n=1}^{\infty} \mathrm{Im}\,\left\{\Phi\left(\frac{n\pi}{R}\right)\right\} \sin\frac{n\pi}{R}x\right] \end{aligned} \tag{16}$$

By termwise integration of the pdf, we obtain the probability P the output is positive [20]:

$$\begin{aligned} P &= \int_0^{\infty} p(x)dx \\ &= \frac{1}{2} + \frac{2}{\pi} \sum_{n=1,3,5,\ldots}^{\infty} \frac{1}{n}\, \mathrm{Im}\,\left\{\Phi\left(\frac{n\pi}{R}\right)\right\} \end{aligned} \tag{17}$$

First, P_F under the given threshold coefficient k is evaluated on the condition that all cells are filled with clutter with parameters of ν_c and β_c. According to the discussion in Sect. 2.4, the statistics for target-detection circuit z^t is expressed by a gamma distribution with the parameters shown in Eqs. (7), (9), and (10) as

$$\begin{aligned} \langle z_i^t \rangle &= (l+1)\langle y \rangle = (l+1)\,\nu_c \beta_c \\ \mathrm{var}\,(z_i^t) &= \mathrm{var}\,(y)\left\{(l+1) + 2\sum_{i=1}^{l}(l+1-i)\,\rho_i^c\right\} \\ &= \left\{(l+1) + 2\sum_{i=1}^{l}(l+1-i)\,\rho_i^c\right\} \nu_c \beta_c^2, \end{aligned}$$

where ρ_i^c is the clutter autocorrelation function (ACF). Then, the scale parameter β_1 and the shape parameter ν_1 are

$$\begin{aligned} \beta_1 &= \frac{(l+1) + 2\sum_{i=1}^{l}(l+1-i)\,\rho_i^c}{l+1} \cdot \beta_c \\ \nu_1 &= \frac{(l+1)\,\nu_c \beta_c}{\beta_1}, \end{aligned} \tag{18}$$

and the chf is $\Phi_1(\omega) = (1 - j\omega\beta_1)^{-\nu_1}$. On the other hand, the statistics of clutter-detection circuit output z^c is obtained considering cells with interrupted succession. The scale parameter β_2 and the shape parameter ν_2 are shown as Eq. (19), and the chf is $\Phi_2(\omega) = (1 - j\omega\beta_2)^{-\nu_2}$. Because $z = z^t - z^c$, the chf of the CFAR output $\Phi_F(\omega)$ is

$$\begin{aligned} \Phi_F(\omega) &= \langle e^{j\omega(z^t - z^c)} \rangle = \langle e^{j\omega z^t} \rangle \langle e^{j(-\omega) z^c} \rangle \\ &= \Phi_1(\omega)\, \Phi_2(-\omega) \end{aligned}$$

$$\beta_2 = \frac{(m-l) + \sum_{i=1}^{m/2}(m-2i)\rho_i^{\mathrm{c}} + \sum_{i=l+2}^{m/2+l+1}(i-l-1)\rho_i^{\mathrm{c}} + \sum_{i=m/2+l+2}^{m+l}(m+l+1-i)\rho_i^{\mathrm{c}}}{m-l} \cdot k\beta_{\mathrm{c}},$$
$$\nu_2 = \frac{(m-l)\,k\,\nu_{\mathrm{c}}\beta_{\mathrm{c}}}{\beta_2} \tag{19}$$

$$= (1 - j\omega\beta_1)^{-\nu_1} \cdot (1 + j\omega\beta_2)^{-\nu_2} \tag{20}$$

Substituting Eqs. (18)–(20) into Eq. (17), we obtain P_{F} under the coefficient k.

Next, we evaluate P_{D}. The target signal and the clutter are independent, therefore the statistics of the superposition of target signal RV X^{t} on clutter RV X^{c} can be written as $\langle X^{\mathrm{t}}+X^{\mathrm{c}}\rangle = \langle X^{\mathrm{c}}\rangle + \langle X^{\mathrm{t}}\rangle$ and $\mathrm{var}\,(X^{\mathrm{t}}+X^{\mathrm{c}}) = \mathrm{var}\,(X^{\mathrm{t}}) + \mathrm{var}\,(X^{\mathrm{c}})$. For obtaining P_{D}, we assume the target signal fills with the target detection cells and does not spill over the clutter detection cells. The scale parameter β_3 and the shape parameter ν_3 when the target is present is obtained using simple substitutions of variables in Eq. (18):

$$\beta_3 = \frac{(l+1) + 2\sum_{i=1}^{l}(l+1-i)\rho_i^{\mathrm{t}}}{l+1} \cdot \beta_{\mathrm{t}},$$
$$\nu_3 = \frac{(l+1)\,\nu_{\mathrm{t}}\beta_{\mathrm{t}}}{\beta_3}, \tag{21}$$

where ρ_i^{t} is the ACF of the target signal, and the chf is $\Phi_3(\omega) = (1 - j\omega\beta_3)^{-\nu_3}$. Then, the chf of the CFAR output $\Phi_{\mathrm{D}}(\omega)$ is

$$\begin{aligned}\Phi_{\mathrm{D}}(\omega) &= \langle e^{j\omega(z^{\mathrm{t}}-z^{\mathrm{c}})}\rangle = \langle e^{j\omega z^{\mathrm{t}}}\rangle\langle e^{j(-\omega)z^{\mathrm{c}}}\rangle \\ &= \{\Phi_1(\omega)\,\Phi_3(\omega)\}\,\Phi_2(-\omega) \\ &= (1 - j\omega\beta_1)^{-\nu_1} \cdot (1 + j\omega\beta_2)^{-\nu_2} \cdot \\ &\quad (1 - j\omega\beta_3)^{-\nu_3}\end{aligned} \tag{22}$$

Substituting Eqs. (18), (19), (21), and (22) into Eq. (17), we obtain P_{D}.

The required SCR is evaluated by the ratio of target power and background objects power at the same false alarm probability and at the same detection probability. The procedures for obtaining the required SCR for the proposed CFAR is as follows:

1. Assume β_{c}, say $\beta_{\mathrm{c}} = 1$.
2. Search k to satisfy the desired P_{F} with Eqs. (17)–(20).
3. Derive β_{t} to satisfy the desired P_{D} with Eqs. (17)–(19), (21) and (22).
4. Obtain the required SCR from $\nu_{\mathrm{t}}\beta_{\mathrm{t}}/(\nu_{\mathrm{c}}\beta_{\mathrm{c}})$.

We have assumed the number of cells for the target detection part is corresponded to the size of a target. If the target detection part does not coincide with the target, the loss occurs. If the target length is, say, half of the length of the target detection part, the SCR reduces by 3 dB.

For qualitatively understanding, Fig. 5 shows the conventional CFAR and the proposed CFAR with computer-generated gamma-distributed random numbers. Clutter power (a) and target power (b) are added to obtain CFAR input (c). The proposed CFAR detected the target clearer than the conventional CFAR did. In the simulation, a higher k in Figs. 1 and 4 was chosen to display the effect of the conventional CFAR and the proposed CFAR.

4. Numerical Result

4.1 Autocorrelation Assumptions for Target and Clutter Signals

There are few reports on experimental ACFs for automotive radars and the exact ACF model is not available now. For evaluating the required SCR for target detection at given P_F and P_D, the required SCRs are compared for several ACF models shown in Fig. 6. For the uncorrelated model shown in Fig. 6(a), the ACF ρ_i is defined by

$$\rho_i = \begin{cases} 1 & \text{for } i = 0, \\ 0 & \text{otherwise.} \end{cases}$$

The exponential correlation model, as shown in Fig. 6(b), was suggested for sea clutter in [18]. The ACF is

$$\rho_i = e^{-\alpha i},$$

where α is the correlation gradient. For a large *alpha*, the model approaches to the uncorrelation model. The ACF for step correlation, as shown in Fig. 6 (c), is

$$\rho_i = \begin{cases} 1 & \text{for } 0 \le i \le \tau, \\ 0 & \text{otherwise,} \end{cases}$$

where τ is the correlation length.

It is possible to independently choose ACF models for the target and clutter. In the evaluation, however, the same ACF model is employed for both target and clutter, because the target and the clutter would have the same dimension in automotive environments.

4.2 The Required SCR

First of all, the uncorrelation model and the exponent correlation model with $\alpha = 1$ are examined for evaluating the proposed method. P_{D} of 0.95 and P_{F} of 10^{-5} are chosen as typical values through the evaluation [2]. The required SCRs

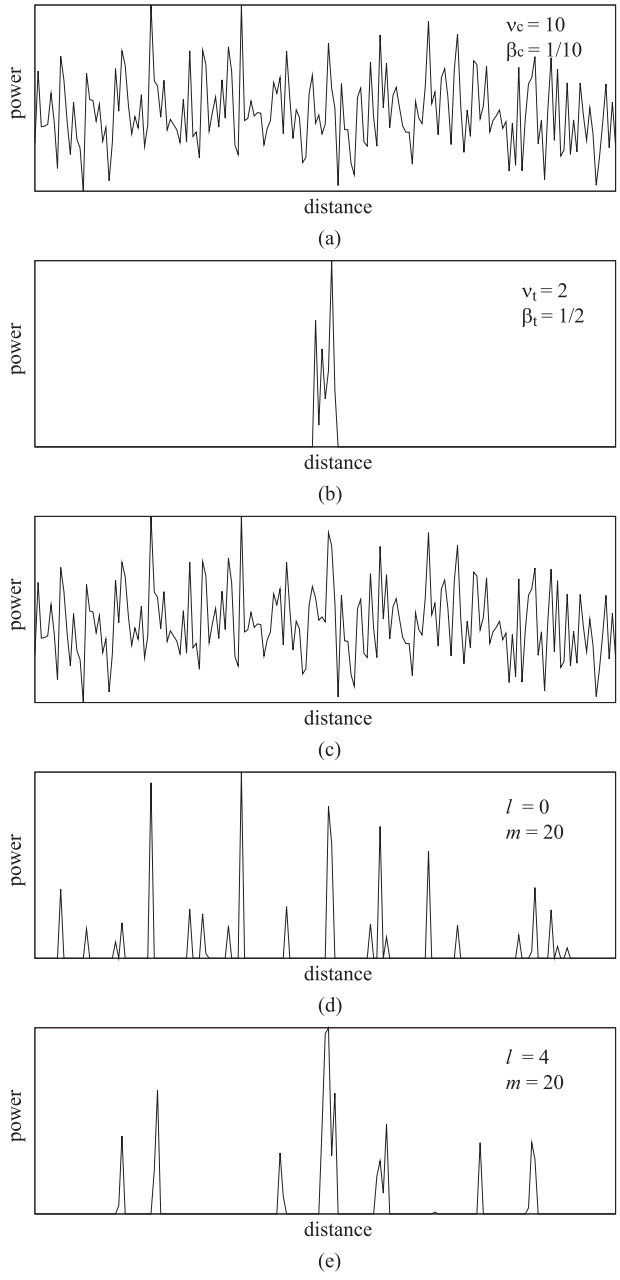

Fig. 5 Computer simulation with gamma-distributed random numbers: (a) clutter signal, (b) target signal, (c) CFAR input (superposition of target and clutter), (d) conventional CFAR result, and (e) proposed CFAR result.

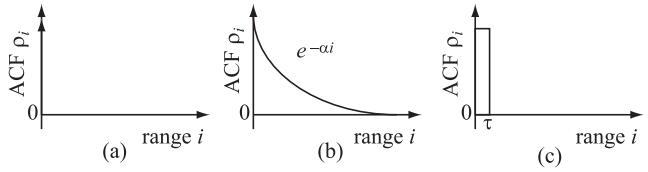

Fig. 6 Possible ACF models for ground clutter and targets in automotive environments: (a) the uncorrelation model, (b) the exponent correlation model, and (c) the step correlation model.

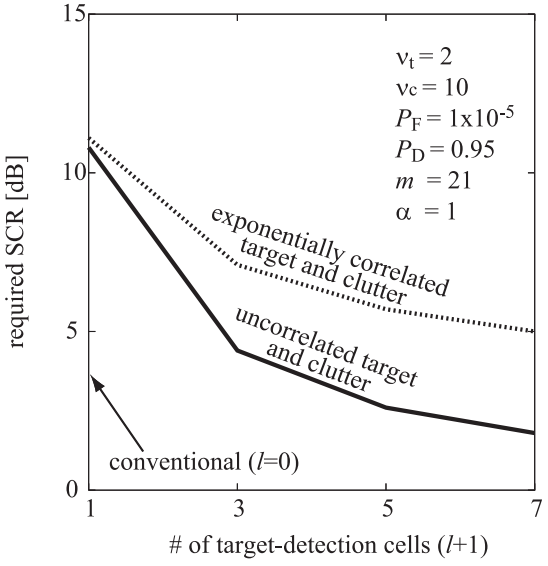

Fig. 7 The required SCR where there are directive reflection targets and the rather constant clutter.

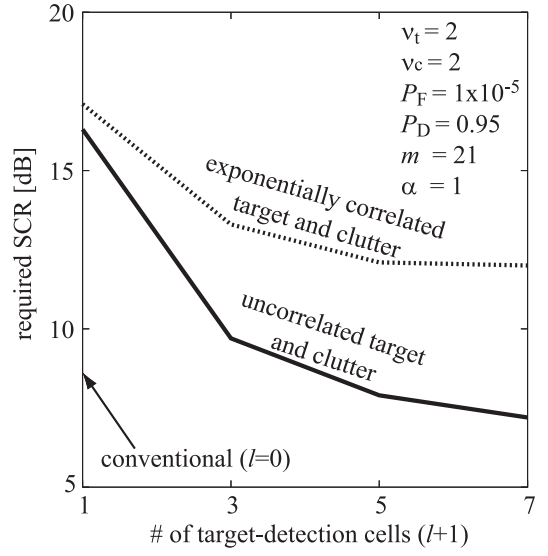

Fig. 8 The required SCR where there are directive reflection targets and clutter.

are calculated for various l and are plotted in Fig. 7. We assume the number of the total CFAR cells of 21 ($m = 20$), and the value is commonly used for CA-CFAR [2]. We also assumes parameters of $\nu_c = 10$ and $\nu_t = 2$, where we assumes targets having directive reflections and clutter having rather constant reflection. The required SCR of the conventional CFAR ($l = 0$) was 10.8 dB and the SCR of the proposed CFAR with the two alongside cells ($l = 2$) for target detection was 4.4 dB. Therefore, proposed CFAR with two alongside target cells improved the required SCR by 6.4 dB, in exchange for a slight resolution degradation. This is because the multiple detection cells reduced the range-by-range target variations. The required SCR for the exponent correlation model is also plotted in Fig. 7. The correlation increased the required SCR, because the correlation increases

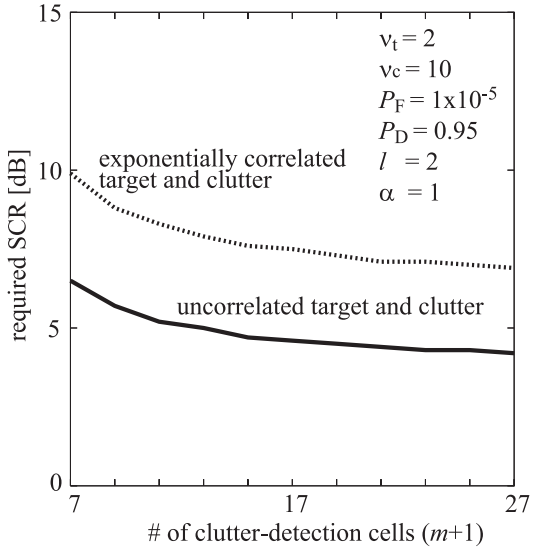

Fig. 9 Dependence of m on the required SCR.

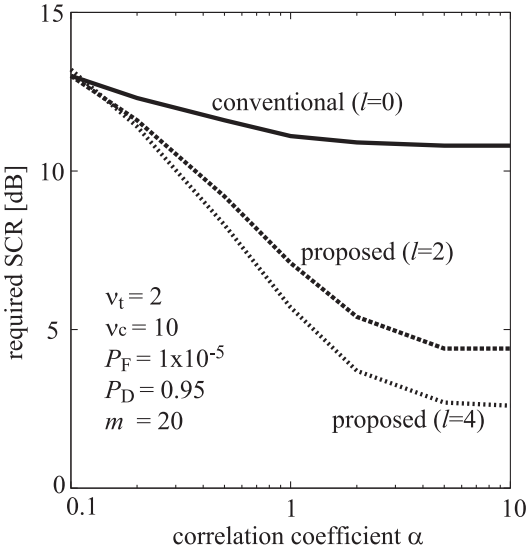

Fig. 11 The required SCR dependence of the correlation gradient in the exponential ACF model.

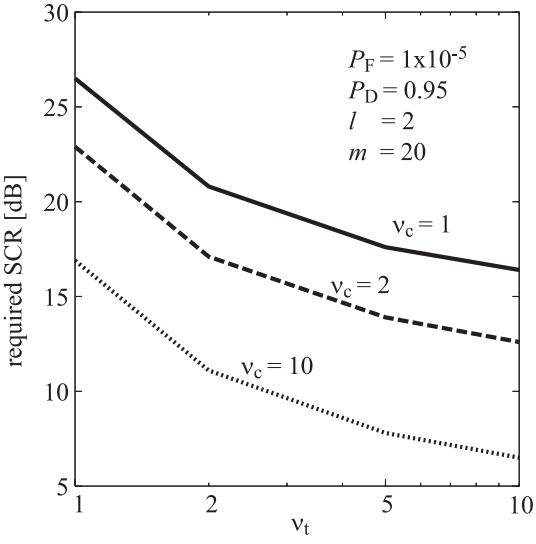

Fig. 10 Dependence of ν_t on the required SCR for various ν_c.

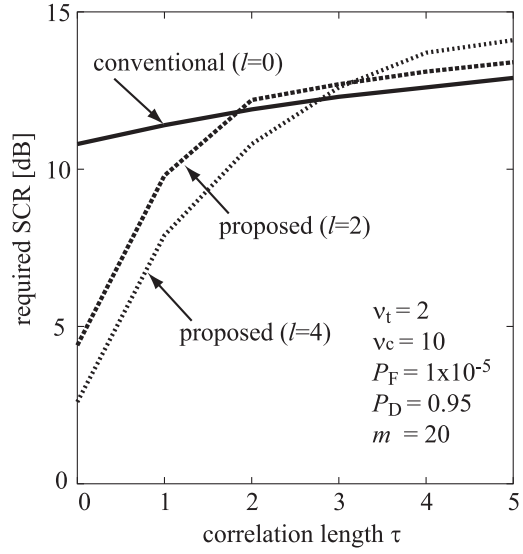

Fig. 12 The required SCR dependence of the correlation length in the step ACF model.

P_F. Even in the correlation model, the proposed CFAR provided a lower required SCR. The proposed CFAR with the two alongside cells improved the required SCR by 4.0 dB.

A required SCR for directive reflections of both targets and clutter ($\nu_t = 2$ and $\nu_c = 2$) was also obtained and is shown in Fig. 8. For the uncorrelation model, the decrease in ν_c from 10 to 2 increased a required SCR of 16.3 dB for the conventional CFAR and 9.7 dB for the proposed CFAR with $l = 2$. A smaller ν_t and a smaller ν_c increased the required SCR, because both the target and clutter signals varied range-by-range. The correlation also degraded the SCRs of both of the conventional and proposed CFAR, and the improvement was 3.8 dB.

Dependence of the number of the entire cells m of the CFAR circuit on the required SCR is shown in Fig. 9. An increase in m decreased the required SCR, but the decrease becomes small for a certain m, say $m = 20$: the required SCR difference between $m = 18$ and $m = 20$ was only 0.1 dB for the uncorrelated case, though the difference between $m = 6$ and $m = 8$ was 0.8 dB.

Dependence of ν_t on the required SCR for the proposed CFAR with $l = 2$ is plotted in Fig. 10 for various ν_c. The required SCR increased as the decreased both in ν_c and ν_t. The proposed CFAR with multiple target detection cells reduced the required SCR. In the evaluation, the uncorrelation ACF model was used as an example.

4.3 Effect of ACF Models on the Required SCR

Effect of ACF models on the required SCR is evaluated. P_D

of 0.95, P_F of 10^{-5}, ν_t of 2, ν_c of 10, and m of 20 are also assumed. Figure 11 shows the required SCR for various correlation gradient in the exponent ACF model. The required SCRs for $\alpha = 10$ are almost the same as ones for the uncorrelation ACF model. On the other hand, the improvement due to the proposed CFAR diminished for a smaller correlation gradient as $\alpha = 0.1$. The proposed CFAR could reduce the required SCR for a larger correlation gradient, and the improvement approached to the uncorrelation model one for $\alpha > 7$.

The required SCR for the step correlation model is also calculated and is shown in Fig. 12. In the figure, $\tau = 0$ means the uncorrelation model. The required SCR rapidly increased as an increase in τ. Especially for a longer τ than l, the required SCR of the proposed CFAR exceeded that of the conventional CFAR. A longer τ increases the power of the clutter detection cells and reduces the power of the target detection cells, and it results in the higher SCR.

5. Conclusion

A CFAR circuit that equipped the target detection part, as well as the clutter detection part, was proposed for future high-resolution short-range automotive radars. An HRR working in automotive environments triggers a higher false alarm probability because the dimensions of target, background objects, and the radar resolution are the same, and it leads to range-by-range signal variations. The required SCR increases with the increase in the false alarm probability. Effect of correlating target and clutter was also considered in the evaluation, because the target and clutter would occupy several range cells and it resulted in a higher SCR.

The proposed CFAR could reduce the required SCR because the target detection cells reduced the range-by-range variations of targets, as well as the clutter detection cells the conventional CFAR had reduced. The proposed CFAR used the squared-law circuit to express the radar signal in power and assumes the range-by-range pulse integration.

The detection performance was evaluated by the required SCR. Comparing it with the conventional CFAR, the proposed CFAR reduced the required SCR by 6.4 dB for the uncorrelation case. The dependence of autocorrelation function on the required SCR was also evaluated on the assumptions for the uncorrelation model, the exponent correlation model, and the step correlation model. An increase in signal correlation of range cells increased the required SCR, but the required SCR of the proposed CFAR was lower than the required SCR of the conventioal CFAR for the correlation gradient of larger than 0.1 in the exponent correlation model. The required SCR of the proposed CFAR of the correlation gradient more than 7 approached the required SCR for the uncorrelation model.

Acknowledgments

This work was supported in part by a Hiroshima City University Grant for Special Academic Research under Grant No. 7112.

References

[1] J. Wenger, "Automotive radar — Status and perspectives," 2005 IEEE Compound Semiconductor Integrated Circuit Symposium (CSIC), pp.21–24, Oct./Nov. 2005.
[2] M.I. Skolnik, Introduction to Radar Systems, 3rd ed., McGraw-Hill, New York, 1980.
[3] J.V. Hubbard, "Digital automatic radar data extraction equipment," J. Brit. IRE, vol.26, pp.397–405, Nov. 1963.
[4] E.K. Al-Hussaini and B.M. Ibrahim, "Comparison of adaptive cell-averaging detectors for multiple target situations," IEE Proc. F., Radar & Signal Process, vol.133, no.3, pp.217–223, 1986.
[5] M. Shor and N. Levanon, "Performances of order statistics CFAR," IEEE Trans. Aerosp. Electron. Syst., vol.27, no.2, pp.214–224, March 1991.
[6] L. Zhao, W. Liu, J.S. Fu, and X. Wu, "A novel approach for CFAR processors design," IEEE Radar Conference, pp.284–288, Atlanta, May 2001.
[7] D. Kok and J.S. Fu, "Signal processing for automotive radar," IEEE Radar Conference, pp.842–846, May 2005.
[8] E. Jakeman and P.N. Pusey, "A model for non-Rayleigh sea echo," IEEE Trans. Antennas Propag., vol.AP-24, no.6, pp.806–814, Nov. 1976.
[9] G.M. Dillard and C.E. Antoniak, "A practical distribution-free detection procedure for multiple-range-bin radars," IEEE Trans. Aerosp. Electron. Syst., vol.AES-6, pp.629–635, Nov. 1970.
[10] M. Sekine, T. Musha, Y. Tomita, and T. Irabu, "Suppression of Weibull-distributed clutters using a cell-averaging LOG/CFAR receiver," IEEE Trans. Aerosp. Electron. Syst., vol.AES-14, no.5, pp.823–826, Sept. 1978.
[11] J. Li and T. Talty, "Channel characterization for ultra-wideband intra-vehicle sensor networks," Military Communications Conference (MILCOM) 2006, pp.1–5, Oct. 2006.
[12] E. Jakeman and R.J.A. Tough, "Non-Gaussian models for the statistics of scattered waves," Advances in Physics, vol.37, no.5, pp.471–529, 1988.
[13] V. Anastassopoulos, G. Lampopoulos, A. Drosopoulos, and M. Rey, "High resolution radar clutter statistics," IEEE Trans. Aerosp. Electron. Syst., vol.35, no.1, pp.43–60, Jan. 1999.
[14] H.J. Muller, "Characterization of radar clutter by gamma induced distributions," Proc. IEEE International Geoscience and Remote Sensing Symposium (IGARSS'98), pp.1216–1218, July 1998.
[15] S. Watts, "Radar detection prediction in k-distributed sea clutter and thermal noise," IEEE Trans. Aerosp. Electron. Syst., vol.AES-23, no.1, pp.40–45, Jan. 1987.
[16] A. Papoulis, Probability, Random Variables, and Stochastic Processes, 3rd ed., WCB McGraw-Hill, Boston, 1991.
[17] F.E. Nathanson, J.P. Reilly, and M.N. Cohen, Radar Design Principles: Signal Processing and the Environment, 2nd ed., Scitech Publishing, Raleigh, North Carolina, 1999.
[18] S. Watts and K.D. Ward, "Spatial correlation in K-distribution sea clutter," IEE Proc., vol.134, Pt.F, no.6, Oct. 1987.
[19] R. Barakat, "First-order statistics of combined random sinusoidal waves with applications to laser speckle patterns," Optica Acta, vol.21, no.11, pp.903–921, Nov. 1974.
[20] S. Takahashi, T. Kobayashi, K. Kage, K. Takahashi, and H. Masui, "Stochastic prediction of transmission performance in mobile communication systems employing anti-multipath techniques in urban propagation environments," IEICE Trans. Commun., vol.E82-B, no.12, pp.1987–1996, Dec. 1999.

Satoshi Takahashi received M.E. and Ph.D. degrees from Tokyo Denki University, Japan, in 1992 and 2001. In 1992, he joined Hitachi, Ltd., where he engaged in research on radio propagation for indoor cordless systems. During 1996–1999, he was a research engineer at YRP Key Tech Labs, Co., Ltd., where he engaged in research on radio propagation for the future 4th generation radio communication systems. Then he conducted the measurement campaigns in metropolitan Tokyo areas at frequencies of 3.35 GHz, 5.20 GHz, 8.45 GHz, and 15.75 GHz with a bandwidth of 100 MHz. In 2002, he joined a national laboratory, Communications Research Laboratory (now National Institute of Information and Communications Technology), where he engaged in intelligent transport systems (ITS) and future radio communication systems. Since 2005, he is an associate professor at Hiroshima City University, Japan. Dr. Takahashi is a member of IEEE and IPSJ.